



Influence of local stress concentrations on the crack propagation in complex welded components

C. Fischer, W. Fricke

Hamburg University of Technology, Institute of Ship Structural Design and Analysis, Hamburg, Germany
w.fricke@tuhh.de

ABSTRACT. While a long stable crack propagation phase was observed during experiments of complex welded components, very conservative assessments of the fatigue life were achieved in the past. The difference was explained by the stress gradient occurring over the plate thickness. This paper deals with numerical crack propagation simulations which were performed for different geometrical variants. The variants differ related to global geometry, boundary conditions and weld shape. The analyses aim to investigate how the crack propagation is altered if the structural configuration gets more complex. In conclusion, the stress gradient over the plate thickness, the apparent plate thickness and the notch effect slows down the crack propagation rate if the same stress value being effective for fatigue appears at the weld toe. Thereby, the load-carrying grade of the weld, the weld flank angle and the geometrical configuration have an impact on both the notch effect and the local stress concentration.

KEYWORDS. Crack propagation simulation; Fatigue life; Notch effect; Stress gradient.

INTRODUCTION

Complex welded components can have hot-spots showing high local stresses with steep stress gradients. These could be critical with respect to fatigue. An example is the three-dimensional intersection of plates shown as variant 5 in Fig. 1. Different variants of this detail were experimentally investigated by means of both large-scale and small-scale fatigue tests over the last decades, see e.g. [2, 11-15]. Dijkstra *et al.* [2] observed an early crack initiation, but a long period of stable crack propagation until the crack had grown through the loaded plate.

However, very conservative fatigue assessments were discovered applying the common fatigue approaches to complex structures, see e.g. [6, 7]. Lotsberg and Sigurdsson [14] explained the disagreement by the stress gradient over the plate thickness which was not covered by the fatigue approach they had selected. Fischer and Fricke [5] established three additional reasons: the apparent plate thickness, the load-carrying grade of the weld and bending constraints of the detail. They supposed correction factors to account for these influences in the fatigue assessment. Generally, the approaches are based on the analysis of tests of small-scale specimens with more or less simple welded joints. Here, no three-dimensional complex stress distribution is on hand.

This paper deals with different crack propagation analyses at both simple joints and complex welded structures in order to investigate further effects, besides the stress gradient, which affects the crack propagation, shape and fatigue life. At first, a comparison of a transverse attachment and its geometrical modifications with the intersection of plates is presented. Four effects which are identified on the basis of different stress distributions and geometry are validated by numerical and analytical crack propagation analyses. In the next step, the geometry is modified to vary the notch effect and the stress

concentration at the weld toe which depend on the load-carrying-grade of the weld, the weld flank angle and the layout of the intersecting plates.

CASE STUDY

Selected Variants

The two-sided transverse attachment (variant 1 in Fig. 1) under axial loading represents a simple welded joint. A crack would be initiated at one of the weld toes and would run through the loaded plate. The complex structure (variant 5) is the intersection of various plates joined by fillet welds. Here, the local hot-spot at the intersection point is critical since a crack would initiate at the weld toe on the surface of the horizontal plate in the loading condition shown. The other three variants are ‘intermediate’ geometries to separate the effects on crack propagation. They are described and used in the following.

Corresponding three-dimensional finite element (FE) models taking advantage of the vertical symmetry plane were created in ANSYS® 13.0. The models consist of solid elements with quadratic shape function (SOLID186), and the welds were completely modelled in order to account for the local stiffness. The models are 200 mm long, 100 mm wide and 70 mm high. No axial and angular misalignments are present and only the critical weld toe was rounded by a radius $r_{ref} = 1$ mm for the determination of the stress field.

The vertical nodal displacements of variants 1 and 5 were suppressed at the bottom. On the symmetry plane corresponding boundary conditions were applied, and the transverse nodal displacement was coupled on the opposite side to represent adjacent structures. The front and back face were loaded by uniform, axial stresses, whereas the axial nodal displacements were suppressed at the back face of the complex structure.

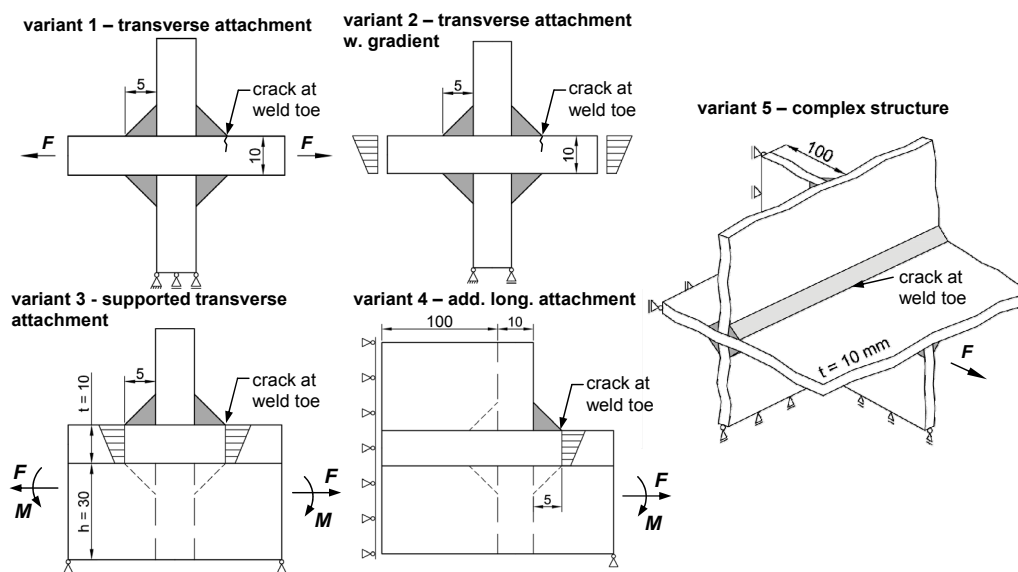


Figure 1: Selected geometrical variants (variants 1 to 4 are cut in the symmetry plane).

Structural Hot-Spot Stress and Effective Notch Stress

Both stresses are commonly used for fatigue assessment of welded joints (see e.g. [10]) and are the basis for comparing the variants. The structural hot-spot stress (HSS) σ_s which appears in front of the rounded weld toe on the symmetry plane consists of the sum of the membrane stress σ_m and bending stress σ_b . Both σ_m and σ_b are determined by linearizing the axial stress component over the plate thickness $t = 10$ mm according to [10]. Moreover, Dong [3] characterized a stress gradient occurring over the plate thickness by means of the degree of bending δ , Eq. (1). Here, $\delta = 0$ denotes pure axial loading and $\delta = 1$ pure bending.

$$\delta = \frac{\sigma_b}{\sigma_m + \sigma_b} \quad (1)$$

The effective notch stress σ_{eff} accounts for the notch effect and the microstructural support of notches by means of rounding the weld toe or the weld root by a radius $r_{\text{ref}} = 1 \text{ mm}$, see [8]. The highest 1st principal stress on that radius is assumed to be effective for fatigue assessment. The effective notch stress is linked with σ_s by the weld shape factor K_W , Eq. (2), which considers the load-carrying grade of the weld and the local weld geometry.

$$\sigma_{\text{eff}} = K_W \sigma_s \quad (2)$$

Comparison of Stress Distributions

In order to reach the same structural HSS $\sigma_s = 176 \text{ MPa}$ at the transverse attachment (1) and the complex structure (5), different levels of nominal stresses were required. A uniform axial loading of 100 MPa was sufficient at variant (5) because of the significant stress concentration at the hot-spot which is illustrated by the calculated distributions of the 1st principal stress in Fig. 2.

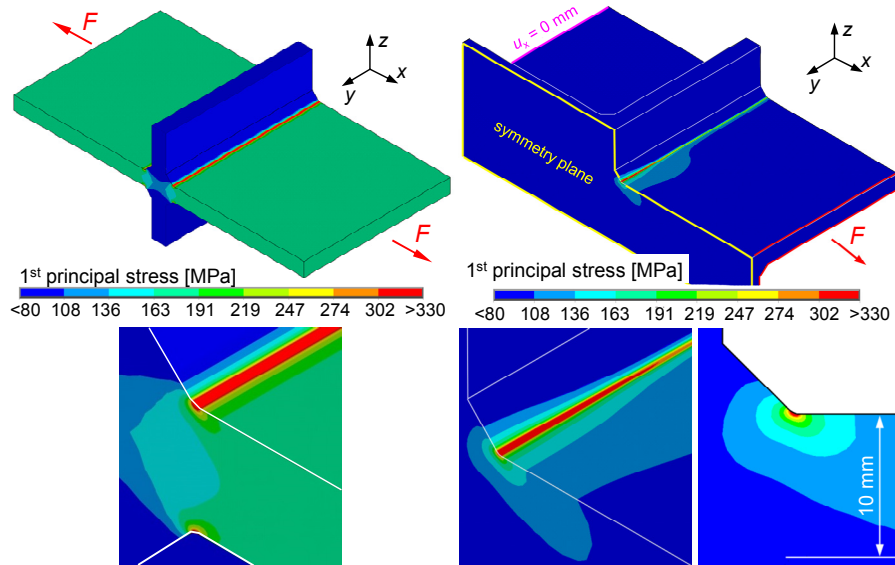


Figure 2: Calculated stress distribution at the transverse attachment (left) and the complex structure (right).

Moreover, the stress distribution over the plate thickness is symmetric in case of transverse attachment (1) due to the weld toe on the opposite side, whereas the stress decreases monotonically for the complex structure (5). These characteristics were represented by different degrees of bending being $\delta = 0$ for variant 1 and $\delta = 0.315$ for the other. While the stress level is constant over the whole width of the transverse attachment (1), it decreases in variant 5 at first significantly and then slows down when the distance from the symmetry plane rises.

The longitudinal plates of the complex structure cause differences as well. The lower plate increases the apparent plate thickness in the symmetry plane; i.e. the cross section is significantly larger than for the transverse attachment. The upper plate affects the load-carrying grade and the level of the effective notch stress. Moreover, the vertical support of the lower longitudinal plate results in a bending constraint which is also found in large plated structures.

'Intermediate' Variants

Three additional variants 2 to 4 according to Fig. 1 were defined for the following crack propagation simulation so that the effects on crack propagation life can be separated. In variant 2, the transverse attachment is loaded such that $\delta = 0.315$ occurs at the weld toe, while variant 3 is modified by a longitudinal plate below the main plate. The plate is 10 mm thick and 30 mm high. The degree of bending $\delta = 0.315$ in the plate is realized by appropriate axial and bending loads. An additional longitudinal plate, having a length $L = 100 \text{ mm}$, is added behind the upper transverse attachment in variant 4. Due to adjusted loads, the degree of bending is $\delta = 0.315$ again.

This longitudinal plate increases the load-carrying grade of the welded joint and also the stress concentration in the symmetry plane. This led to a similarly high stress decrease along the weld line as for the complex structure. The



difference between variant 4 and 5 is only the support of the lower longitudinal plate changing also the kind of loading, but not σ_s or σ_{eff} and δ at the hot-spot.

COMPUTED FATIGUE LIVES

Crack Propagation Analysis

A half-circular initial crack is assumed at the critical weld toe for all variants. The crack initiation phase was considered by choosing a small initial crack length $a_i = 0.15$ mm. The crack growth increments da and dc were computed for a defined number of cycles dN via individual integrations of the law by Paris and Erdogan [16]:

$$\frac{da}{dN} = C (\Delta K_{I,a})^m \quad (3)$$

Eq. (3) links the crack propagation rate da/dN to the range of the stress intensity factor (SIF) $\Delta K_{I,a}$ at the deepest point of the crack by using the material parameter $C = 3 \cdot 10^{-13}$ and $m = 3$ (unit: N and mm). The integrations, however, must be done discretely because the SIF varies non-linearly and depends on the crack depth and crack shape. In order to avoid an under- or overestimation of cycles, the average value of the cyclic SIF was used when the crack grows from one stage (1) to the next (2):

$$\log(\Delta \bar{K}_I) = 0.5 [\log(\Delta K_{I,1}) + \log(\Delta K_{I,2})] \quad (4)$$

A separate block of elements was added to the FE models. It includes half of the semi-elliptical crack shape with half crack depth a and width c . The block was connected with the surrounding model by contact elements transferring all kinds of forces and moments (bonded conditions). The block is 10 mm long and high, whereas the width depends on the actual half crack width c . The 20-node solid elements size $0.1 \cdot a$ at the crack front, and the midsize nodes are shifted to the quarter points towards the crack front to improve the accuracy.

No weld toe radius was considered to simplify the modelling, but this causes an additional stress singularity and a steep increase of the SIF. Due to this, the SIF $K_{I,c}$ at the plate surface was estimated by extrapolating the SIF values computed at the three previous nodes. Generally, K_I at each node along the crack front was determined individually via the J -integral using six contour integrations.

Fischer and Fricke [4] described the modelling of the crack and the estimation of $K_{I,c}$ in detail. They applied the procedure to a load-carrying cruciform joint and obtained a satisfying agreement with experimental results.

	1) Transverse attachment	2) Transverse attachment w. gradient	3) Supported transverse attachment	4) Additional longitudinal attachment	5) Complex structure
Degree of bending δ	0.0	0.315	0.315	0.315	0.315
Final crack depth a_f [mm]	8.48	8.51	8.43	8.44	8.45
Final crack width $2c_f$ [mm]	36.1	49.2	42.3	39.8	38.3
Fatigue life N_p	300,000	385,600	452,200	456,200	509,600
Rel. fatigue life	1.00	1.29	1.51	1.52	1.70

Table 1: Computed fatigue life N_p for the same structural hot-spot stress $\sigma_s = 176$ MPa.

Fatigue Lives Referring to Same Structural Hot-Spot Stress

Between nine and eleven integrations with up to 14 internal loops were performed until the crack had reached the final depth $a_f \approx 8.5$ mm, being close to the opposite plate surface. In this process, smaller increments dN are considered for small cracks.

Fig. 3 shows the evolution of the crack depth of the variants for the same structural HSS $\sigma_s = 176$ MPa. Here, the additional longitudinal attachment (4) is omitted since the crack grows similarly as for the supported transverse



attachment (3). First differences in crack growth occur at a small crack depth $a \approx 0.5$ mm. This corresponds to ca. 10^5 cycles. Afterwards, faster crack propagation can be observed at variants 1 and 2. The curves of the other two variants deviate beyond $a \approx 1.5$ mm.

Finally, the transverse attachment (1) achieves the shortest fatigue life N_p , see also Tab. 1. The next are the transverse attachment with stress gradient over the plate thickness (2), the supported transverse attachment (3), and, finally, the complex structure (5). Tab. 1 also lists in the last line the relative fatigue life referring to that of variant 1. The largest influence (29%) is caused by the stress gradient over the plate thickness (2). Both the apparent plate thickness (3) and the bending constraint (5) increase N_p by about 12%, compared with the previous variants.

It is worth noting that the stress gradient along the weld line does not affect the life since the same N_p is computed for variants 3 and 4. Although the two variants differ with respect to the load-carrying grade of the weld, the same stress distribution over the plate thickness occurs. The gradient along the weld line, however, has an impact on the aspect ratios of the crack, see Tab. 1. The final ratio is relatively small at variant 2 because the stress level is constant along the weld line, whereas the level decreases over the plate thickness. The final aspect ratio increases from the supported transverse attachment (3) to the complex structure (5) as the stress gradient along the weld line gets more pronounced and slows down the crack growth in this direction.

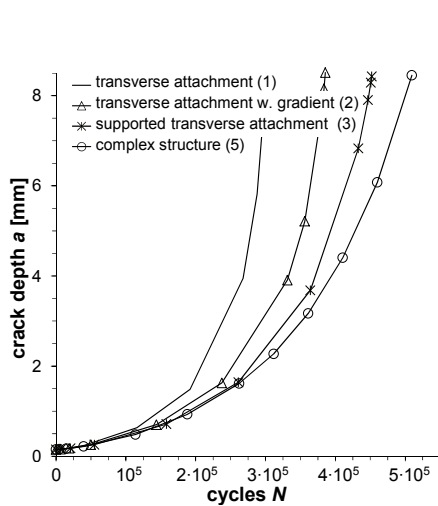


Figure 3: Determined crack depth vs. applied cycles.

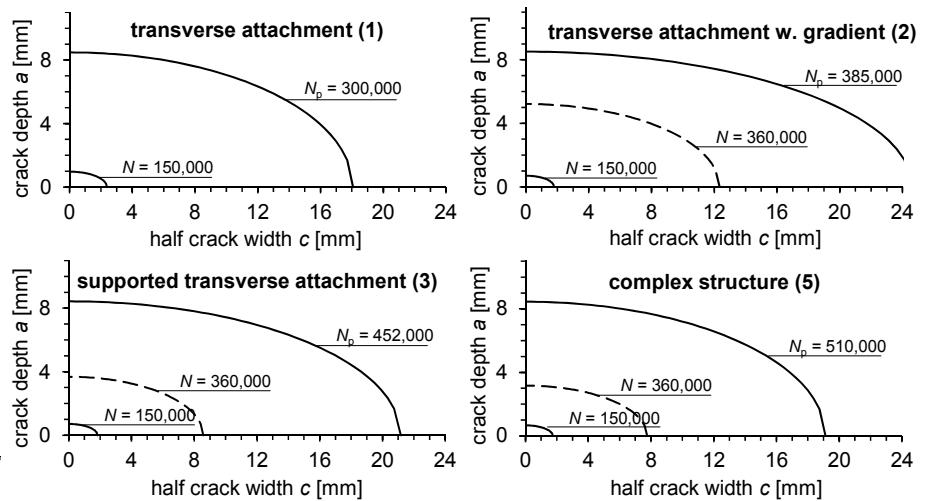


Figure 4: Calculated crack shapes for variants 1 to 3 and 5.

	1) Transverse attachment	2) Transverse attachment w. gradient	3) Supported transverse attachment	4) Additional longitudinal attachment	5) Complex structure
Weld shape factor K_W	2.41	2.24	2.17	2.35	2.43
Fatigue life N_p	297,000	308,500	329,000	418,700	515,000
Rel. fatigue life	1.00	1.04	1.11	1.41	1.73

Table 2: Computed fatigue life N_p for the same effective notch stress $\sigma_{eff} = 425$ MPa.

This influence is also visible when comparing the crack shapes for defined number of cycles, see Fig. 4 showing half crack shapes of variant 1 to 3 and 5 for the same number of cycles ($N_p = 150,000$; $N_p = 360,000$ and at final life) and $\sigma_s = 176$ MPa. The transverse attachment (1) does not reach $N_p = 360,000$ since it has the highest crack propagation rate. While the crack shapes of the variants are almost similar for $N_p = 150,000$, after this they start to differ obviously between the simple transverse attachments (1 and 2) and the more complex variants 3 and 5. Nevertheless, semi-elliptical crack shapes evolve in all cases and the more effects are present, the smaller the computed crack size is.

Fatigue Lives Referring to Same Effective Notch Stress

The computed life can be converted by adjusting the load level in order to consider the same effective notch stress $\sigma_{eff} = 425.3$ MPa on the radius r_{ref} at symmetry plane, see Tab. 2. Here, the stress gradient over the plate thickness (variant 2) as

well as the apparent plate thickness (variant 3) have only minor influence on fatigue life since the stress concentration factor is smaller for bending loads (see e.g. [17]) and the apparent plate thickness is included in the notch effect by the ratio $r_{ref}/(b+t)$ as defined in Fig. 1.

The lives for the supported transverse attachment (3) and the additional longitudinal attachment (4) differ by about 27% in this comparison. The reason is the load-carrying grade of the fillet weld which is increased by the additional longitudinal attachment. The different load-carrying grades can be seen in the rise of the weld shape factor K_W from 2.17 to 2.34. Its effect on life can be assessed for e.g. the variants 3 and 4 by raising the ratio of K_W to the power of three:

$$\frac{N_{p,3}}{N_{p,4}} = \left(\frac{N_{p,3}}{N_{p,1}} \right) \cdot \left(\frac{K_{W,4}}{K_{W,3}} \right)^3 = 1.41 \quad (5)$$

Here, the first term takes into account the increase with respect to the transverse attachment (1). The assessment agrees well with the computed relative lives of Tab. 2. Moreover, the complex structure reaches even longer life (variant 5 vs. 4), caused by an increased K_W and the bending constraint. In general it can be stated that an increased weld shape factor K_W results in a decreased crack growth due to the lower stress level in the plate.

ASSESSMENT OF THE INDIVIDUAL INFLUENCES

Stress Gradient over Plate Thickness

Analytical crack propagation analyses, in which the degree of bending δ was varied, were carried out for a transverse attachment having the dimensions of variant 1. By starting with a semi-circular initial crack of $a_i = a_i = 0.15$ mm, the life was counted until the crack had reached $a_f = 3$ mm. The following propagation phase was neglected since the aspect ratio was small and the increase in life, too.

The crack growth increments da and dc were again determined individually via the integration of the Paris law. The required SIF for the deepest point and for the surface point were taken from [1]. The stress magnification factors $M_{k,c}$, referring to the surface point, were constant and correspond to the ones for $a = 0.15$ mm as suggested in [1]. The estimated lives were normalized with respect to the case of pure membrane loading ($\delta = 0$). Fig. 5 shows the crack depth as a function of the relative fatigue life for different degrees of bending. An increase of nearly 300% is found for $\delta = 1$, being in agreement with calculations in [14], and of about 30% for $\delta = 0,315$ as in the simulation.

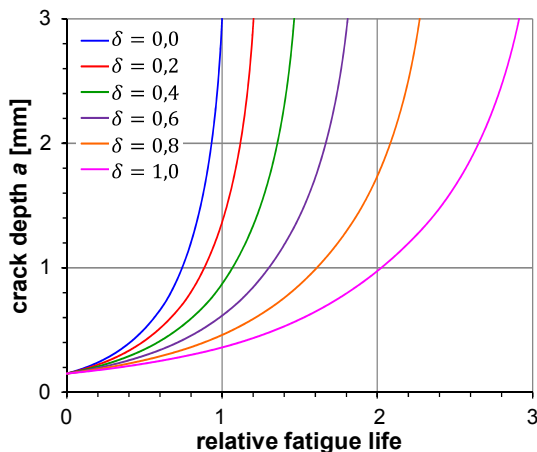


Figure 5: Computed crack depth at transverse attachment with different degrees of bending δ vs. relative fatigue life.

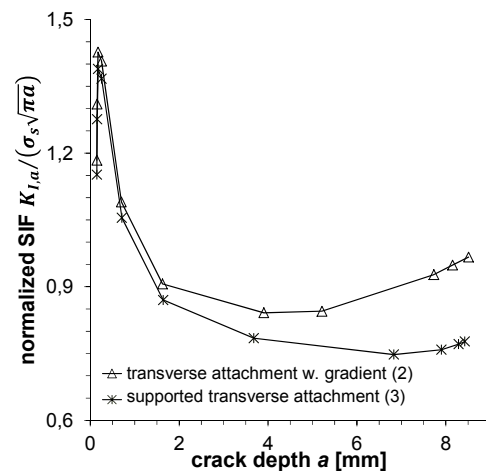


Figure 6: Influence of the remaining cross section on the SIF.

Apparent Plate Thickness

The SIF at the deepest point depends among others on the relative crack depth a/t , the effect of which is described by means of the geometry function. If an additional plate is existent, the apparent plate thickness is increased.

Its influence on crack propagation can be illustrated when normalizing $K_{I,a}$ at the deepest point of variant 2 and 3 by means of the structural stress σ_s , multiplied by $\sqrt{\pi a}$, see Fig. 6. In the beginning, the normalized SIF increases because the semi-circular initial crack becomes flatter (semi-elliptical). With growing crack depth, the stress magnification M_k due to the weld toe notch vanishes and the increased apparent plate thickness gains influence. The SIF of the two variants show increasing deviations for $a > 1$ mm. Smaller values and a slower increase are obtained for the supported transverse attachment (3), leading to an extended life.

In order to assess the effect, the geometry function Y for a single edge crack with $a/c = 0$ in a finite thickness according to Tada *et al.* [18] was integrated discretely from $a_i = 0.15$ mm to $a_f = 8.5$ mm. Different relative heights b/t of the lower longitudinal plates were considered; see Fig. 1 for the definition of b . The influence of the magnification M_k was neglected because differences regarding $K_{I,a}$ and, consequently, the crack growth had been found for $a > 1$ mm, where the M_k factors are no more effective, see [9]. The analytical solution for $b/t = 3$ yields an increase of relative life by about 17% and agrees well with the difference between variant 2 and 3 on the basis of equal structural HSS (Tab. 1).

Modified Notch Effect

The local stress concentration at hot-spots and, consequently, the weld shape factor can be additionally affected by the layout of the transverse attachment and the flank angle α of the weld seam. Hence, the crack propagation is altered. The intersection of a sloped transverse attachment is a typical detail in cargo holds of bulk carriers, see e.g. [6]. Three configurations of the attachment (Fig. 7) are selected in the following. The critical weld toe is always arranged vertically above the weld toe on the opposite side.

At first, the slope is set to 45° (Detail A) and the attachment is shifted so that the flank angle of the critical weld seam remains 45° . Thus, the center lines of the plates intersect each other eccentrically. At Detail B, the center lines are arranged aligned causing a smaller flank angle $\alpha = 25^\circ$. A steeper angle $\alpha = 33^\circ$ occurs with a steeper slope of the transverse attachment and by still aligned center lines, see Detail C in Fig. 7.

For each of the three details, FE models of the variants 1 to 3 and 5, shown in Fig. 1, are generated and crack propagation is simulated using the previously described conditions. The influence of the bending constraint applied to the complex structure (5) is determined approximatively by comparing variant 3 and 5 and considering the changed weld shape factor by Eq. (5) additionally.

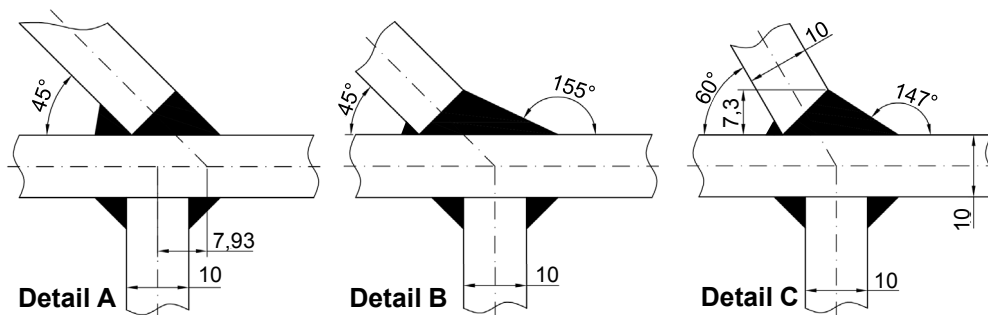


Figure 7: Considered configuration of a sloped upper transverse attachment: with slope angle of 45° and a) eccentric and b) aligned center lines as well as c) with slope angle of 60° and aligned center lines.

	1) Transverse attachment	2) Transverse attachment w. gradient	3) Supported transverse attachment	5) Complex structure
Degree of bending δ	0.0	0.316	0.316	0.316
Weld shape factor K_W	2,36	2,21	2,15	2,39
Final crack depth a_f [mm]	8.45	8.48	8.49	8.51
Final crack width $2a_f$ [mm]	36.1	46.6	44.9	40.1
Fatigue life N_p	283,800	291,200	306,400	505,00
Rel. fatigue life	1.00	1.03	1.08	1.78

Table 3: Computed fatigue life N_p for the same effective notch stress $\sigma_{eff} = 425$ MPa at Detail A.

The results referring to equal $\sigma_{\text{eff}} = 425$ MPa are listed in Tab. 3 to Tab. 5. At Detail A, the calculated final crack shapes as well as the weld shape factors are almost similar to the previous simulations (Tab. 2), despite of the sloped attachment. Additionally, the calculated fatigue lives of the transverse attachment with and without stress gradient (variant 1 and 2) agree with each other. Small deviations, however, are obtained for both the supported transverse attachment (3) and the complex structure (5). Here, the sloped layout affects the stress distributions over the complete cross section on the symmetry plane which can be recognized by the normalized SIF, as illustrated for the two configurations of the supported transverse attachment (3) in Fig. 8. Higher values appear at the eccentric, sloped layout beyond $a > 1.75$ mm and lead to faster crack propagation and shorter life finally.

In Detail B, the weld flank angle is smaller at the same time and reduces the local stress concentration at the weld toe which becomes apparent in generally smaller weld shape factors K_W . Hence, higher external loadings are required for $\sigma_{\text{eff}} = 425$ MPa and the fatigue lives are shorter compared to the other two configurations, see Tab. 2 to Tab. 4. Additionally, the structural hot-spot stresses rise according to Eq. (2) since σ_{eff} is constant and K_W smaller. That effect in conjunction with the lower stress concentration decreases the degree of bending at Detail B. Moreover, the effect of the bending constraint at the complex structure (5) is highly reduced since the relative life rises by only about 21%.

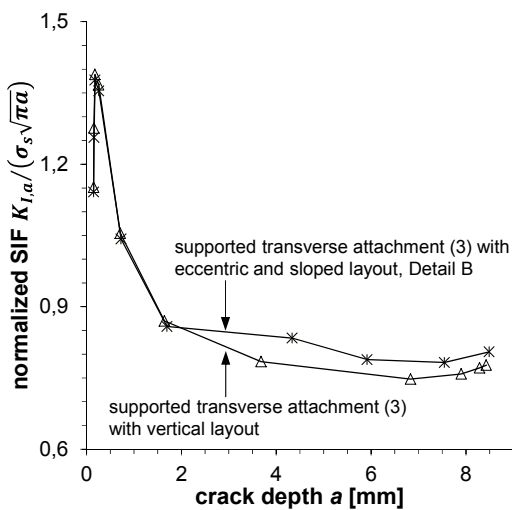


Figure 8: Influence of the layout of the transverse attachment on the SIF.

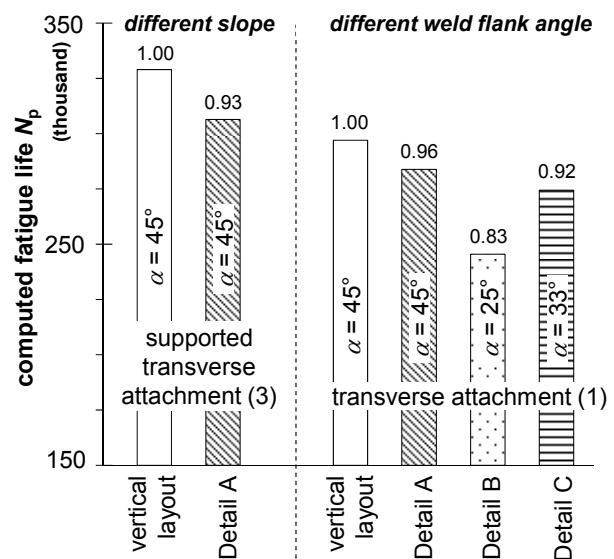


Figure 9: Influence of slope and weld flank angle on fatigue life, shown for selected variants for equal σ_{eff} .

	1) Transverse attachment	2) Transverse attachment w. gradient	3) Supported transverse attachment	5) Complex structure
Degree of bending δ	0.0	0.266	0.266	0.266
Weld shape factor K_W	2,11	2,00	1,93	1,98
Fatigue life N_p	245,500	259,300	266,000	297,000
Rel. fatigue life	1.00	1.06	1.08	1.21

Table 4: Computed fatigue life N_p for the same effective notch stress $\sigma_{\text{eff}} = 425$ MPa at Detail B.

In detail, K_W at the sloped transverse attachment (1) of Detail B, is about 12% smaller compared to the vertical attachment and would shorten fatigue life by about 40% due to increased external loadings. The flatter flank angle, however, compensates the effect partly as the relative lives differ by about 17%. A similar difference is obtained when the effects of the deviating weld shape factors and M_k factors referring to the flank angle are considered. At variant 2, the degree of bending decreases and shortens the fatigue life as shown in Fig. 5.

At the last Detail C, the flank angle modifies the stress distribution over the plate thickness and increases weld shape factors but not as much that they agree with the vertical configuration. Hence, the required level of the external loading is changed and the fatigue lives of the variants are longer than for Detail B but shorter for the other, see Tab. 5, Tab. 4 and



Tab. 2. The different variants of the transverse attachment (variant 1 to 3), both referring to Detail C and the vertical layout, deviate from each other by about 10% being caused by a nearly constant difference between the weld shape factors. Again, the effect of the bending constraint is reduced.

The influence of the flank angle is analytically considered by the stress magnification factor M_k being e.g. reported in the IIW guideline [10]. The integration of M_k from $a_i = 0.15$ mm to $a_f = 3$ mm yields an increasing relative life of about 22% for $\alpha = 25^\circ$ and $a/c = 0$ compared to $\alpha = 45^\circ$. The factor is equal one for crack depths $a \geq 3$ mm and thus ineffective. The increase of life is about 14% for the steeper flank angle $\alpha = 33^\circ$ of Detail C.

Fig. 9 illustrates the influence of the sloped layout and the weld flank angle for two selected variants. The life of the supported transverse attachment (3) decreases at Detail A. The effect is overlaid by the smaller flank angle at the other two details and, hence, omitted. The stress concentration of the transverse attachment (1) is only affected by the flank angle, being smaller at Detail B and C. Thus, the computed life is reduced.

	1) Transverse attachment	2) Transverse attachment w. gradient	3) Supported transverse attachment	5) Complex structure
Degree of bending δ	0.0	0.3	0.3	0.3
Weld shape factor K_w	2.27	2.12	2.04	2.18
Fatigue life N_p	274,500	283,000	296,200	390,100
Rel. fatigue life	1.00	1.03	1.08	1.42

Table 5: Computed fatigue life N_p for the same effective notch stress $\sigma_{eff} = 425$ MPa at Detail C.

		1) Transverse attachment	2) Transverse attachment w. gradient	3) Supported transverse attachment	5) Complex structure
Detail A	fatigue life N_p	304,800	382,000	437,300	521,900
	rel. fatigue life	1.00	1.25	1.43	1.71
Detail B	fatigue life N_p	371,200	457,800	524,700	538,000
	rel. fatigue life	1.00	1.23	1.41	1.45
Detail C	fatigue life N_p	329,100	416,600	491,300	529,600
	rel. fatigue life	1.00	1.27	1.49	1.61

Table 6: Computed fatigue life N_p for the same structural HSS $\sigma_s = 176$ MPa at three sloped configurations.

The influences of both the layout and the flank angle is also directly included in the crack propagation simulation on the basis of the same structural HSS σ_s , see Tab. 1 and Tab. 6, but not in the fatigue assessment using this type of stress. Due to the flatter flank angle at Detail B and C, the absolute fatigue life is increased by about 25% and 11%, respectively. This agrees with the assessment being based on the integrated M_k factor. The relative life of Detail A to C does not rise as much as for the vertically supported transverse attachment (3) because the apparent plate thickness is less effective due to the sloped layout. The different influences are suppressed at the complex structure (5) and nearly same absolute fatigue life is achieved. However, the increase of the relative life is rather different because of the sloped layout.

CONCLUSIONS AND OUTLOOK

The paper presents crack propagation simulations which were performed for different welded geometries – from a transverse attachment up to a complex structure. The determined fatigue lives were compared assuming equal structural HSS and alternatively effective notch stress in all variants. The complex structures showed longer fatigue life due to a higher stress concentration, resulting in changed stress distribution along the crack path. The following conclusion can be drawn:

- Longer crack propagation phase observed in experiments of complex structures can be found also in numerical crack propagation simulation;



- The crack propagation rate at complex structures is slowed down by: the stress gradient over the plate thickness, the apparent plate thickness, the notch effect and the bending constraint of the detail;
- The stress gradient along the weld line does not affect the life but the aspect ratio of the semi-elliptical crack shape;
- The notch effect depends on the load-carrying grade of weld, the flank angle and of the layout of the transverse attachment and it affects the local stress concentration, leading to longer life.

The obtained influences should be investigated for further configurations, varying in particular the thickness of the axially loaded plate as well as of the attachments. This would lead to different local support of the critical weld toe, especially if the thicknesses are different.

REFERENCES

- [1] BS 7910:2005, Guide to methods for assessing the acceptability of flaws in metallic structures, British Standards Institution, London.
- [2] Dijkstra, O., Janssen, G., Ludolph, J., Fatigue tests on large scale knuckle specimens, in: W.-C. Cui, Y.-S. Wu, G.-J. Zhou (Eds.), Proc. 8th Int. Symp. on Practical Design of Ships and Other Floating Structures (PRADS), Elsevier, Amsterdam, (2001) 1145–1151.
- [3] Dong, P., A structural stress definition and numerical implementation for fatigue analysis of welded joints. *Int. J. Fatigue*, 23 (2001), 865–876.
- [4] Fischer, C., Fricke, W., Realistic fatigue life prediction of weld toe and weld root failure in load-carrying cruciform joints by crack propagation analysis., in: C. Guedes Soares, J. Romanoff (Eds.), Analysis and Design of Marine Structures – Proc. 4th Int. Conf. on Marine Structures (MARSTRUCT), Taylor & Francis, London, (2013) 241–248.
- [5] Fischer, C., Fricke, W., Consideration of stress gradient effects for complex structures in local fatigue approaches, in: C. Guedes Soares, R.A. Shenoi (Eds.), Analysis and Design of Marine Structures - Proc. 5th Int. Conf. on Marine Structures (MARSTRUCT), Taylor & Francis, London, (2015).
- [6] Fischer, C., Fricke, W., Rizzo, C.M., N-SIF based fatigue approaches of hopper knuckle details, in: E. Rizzuto, C. Guedes Soares (Eds.), Sustainable Maritime Transportation and Exploitation of Sea Resources, Taylor & Francis, London, (2011).
- [7] Fricke, W., Recommended hot-spot analysis procedure for structural details of FPSO's and ships based on round-robin FE analysis, in: J.S. Chung (Ed.), Proc. 11th Int. Offshore and Polar Engng. Conf. (ISOPE), International Society of Offshore and Polar Engineers, Cupertino, CA, (2001) 89–96.
- [8] Fricke, W., IIW recommendations for the fatigue assessment of welded structures by notch stress analysis, Woodhead Publishing Limited, Cambridge (2013).
- [9] Hobbacher, A., Stress intensity factors of welded joints, *Engng. Fract. Mech.*, 46 (1993) 173–182.
- [10] Hobbacher, A., Recommendations for fatigue design of welded joints and components, Welding Research Council, New York, NY, (2009).
- [11] Iida, K., Matoba, M., Fatigue strength of hold frame ends in ship hulls. International Institute of Welding, IIW-Doc. XIII-950-80, (1980).
- [12] Kang, J., Kim, Y., Heo, J., Fatigue strength of bent type hopper corner detail in double hull structure, in: M.M. Salama, P.K. Gorf, C.F. Mastrangelo, S. Balint (Eds.), Proc. OMAE Specialty Symp. on Integrity of Floating Production, Storage & Offloading (FSPO) Systems, ASME, Houston, TX, (2004).
- [13] Kim, W., Lotsberg, I., Fatigue test data for welded connections in ship-shaped structures, *J. Offshore Mech. and Artic Eng.*, 127 (2005) 359–365.
- [14] Lotsberg, I., Sigurdsson, G., Hot spot stress S-N curve for fatigue analysis of plated structures, *J. Offshore Mech. and Artic Eng.* 128 (2006) 330–336.
- [15] Osawa, N., Fatigue assessment of bilge knuckle joint of VLCC according to JTP / JBP rules, in: Y. Sumi (Ed.), Comparative studies on the evaluations of buckling/ultimate strength and fatigue strength based on IACS JTP and JBP rules, (2005) 3.1–3.5
- [16] Paris, P.C., Erdogan, F., A critical analysis of crack propagation laws, *J. Fluid Engng.* 85, (1963) S. 528–533.
- [17] Peterson, R.E., Stress concentration factors, J. Wiley & Sons, New York, NY, (1974).
- [18] Tada, H., Paris, P.C., Irwin, G.R., The stress analysis of cracks handbook, Del Research Corporation, St. Louis, MO, (1985).